The Spanish Review of Financial Economics

www.srfe.journals.es

# ANALYTICAL STUDY OF URBAN HEAT SPOT PATTERNS IN COLOMBO DISTRICT FROM 1988 – 2019 BASED ON LANDSAT DATA

**SAUMYA CHATHURANGA[a], and CHANDANA JAYARATNE[b]**

[a,b]Department of Physics, University of Colombo, Colombo 00300, Sri Lanka.

**Abstract**

Researching on urban heat island (UHI) is a hot topic among urban designers due to its adverse impacts. This paper focuses on studying spatial and temporal dynamicity of surface UHI in the Colombo district based on correlations between land surface temperatures (LST) with normalized difference vegetation index (NDVI) and normalized difference built-up index (NDBI) using Landsat data from 1988 to 2019. Image processing and statistical analysis were done using QGIS Desktop
3.16.0 and RStudio softwares respectively. The mean of LSTs were continuouslly incerasing during 1988 - 2019. The highest LSTs were observed at the Colombo harbour area in both 1997 and 2007. After initiation of the port city project in 2015, these values have been increased rapidly around the Colombo port city area. The expansion of UHI area was 71.55% between 1988 to 2019 and they were distributed from the western coastal belt to the east along with the central part of the district. The urban hot spots (UHS) were compacted at harbour and port city area. Additionally, new hot spots have been generated since 2017 adjacent to "Seethagama". These small pockets are too hot and not very conducive for human settlements. Parking lots, compacted built-up areas, and ongoing industrial construction areas influence the formation of UHS. Considering this critical situation, it is highly recommended that to move mitigation strategies like urban greening methods, cooling pavements and cooling roofs etc. These results could be used towards a well-designed urban planning system to maintain the ecological balance within the study area.

**Keywords:** Heat island, urban hot spots, LST, NDVI, NDBI.

## INTRODUCTION

Scientists believe the climate has been warming and there are potential impacts of increasing urban heat island (UHI) effect since the 19$^{th}$ century, due to exponential growth of urbanization, industrialization, and environmental issues (Chen et al., 2003; Kim et al., 2005; Tan et al., 2010). UHIs contribute to health risks, high energy demand, and negative effect on the environment. Thus, investigating this scenario has become an essential need of urban planning (Estoque et al., 2017). Landscape with built-up and bare land enhance the effect while water bodies and urban greenness reduce the intensity of UHI (Amiri et al., 2009; Yang et al., 2016; Zhang et al., 2009).

The canopy layer heat island (CLHI), boundary layer heat island (BLHI), and surface urban heat island (SUHI) are three-layer categories of UHIs. The SUHI occurs due to sun heat, roofs and pavement being hotter than the air while shaded surfaces are close to air temperatures (Reducing Urban Heat Islands: Compendium of Strategies Urban Heat Island Basics, 2008; Yuan et al., 2007). Monitoring spatial-temporal changes is the most popular way to observe this phenomenon worldwide (Chen et al., 2006; Li et al., 2006; Manawadu & Liyanage, 2008; Sharma & Joshi, 2014; Sultana Parvin & Abudu, 2017). Remote sensing (RS) technology enables us to investigate the dynamicity of landscape spatial patterns. RS-derived LST (Land Surface Temperature) data have been used to examine UHI characteristics with surface biophysical parameters such as vegetation distribution,

impervious surface, and soil (Guo et al., 2015).
The Landsat project continuously provides high-quality resolution satellite images since 1972. Landsat 5 TM (launched 1984) and Landsat 8 OLI (launched 2013) have been imaging the earth surface in the thermal infrared band with resolution 120m and 100m respectively (Barsi et al., 2006; U.S. Geological Survey, 2016). Researchers developed different algorithms to retrieve LST data from these Landsat imageries such as temperature/emissivity separation method, split-window method, mono-window method, and the single-channel method (Liu et al., 2011).

Urban hot spots (UHS) are recognized as extremely high-temperature areas and these spots generate due to human activities inside urban heat islands (Chen et al., 2006; Coutts et al., 2016; Rodriguez Lopez et al., 2017). Hence, researching these spot patterns is an important task in present urban sustainability planning.

There are more evidence that conclude that Sri Lanka's climate has been changing over decades. Scientists noticed that annual mean air temperature increased by 0.016℃ during 1961-1990, and mean annual precipitation decreased by 144 $mm$ during this period compared to 1931-1960. Furthermore, they predicted mean temperature may be elevated by approximately 0.9-4℃ over baseline (1961-1990) by 2100. Thus, these worming trends verify the elevation of both greenhouse effect and local heat island effect due to rapid urbanization (Gerald et al., 2015). Additionally, the researchers have conducted well-organized UHI investigations regarding Colombo city, Sri Lanka. Emmanuel (2005) discussed that trend of hard land cover reduced the level of thermal comfort, especially during night time, and observed more significant thermal discomfort in the center part of the city than rural areas.

Aim of the Study

In previous studies, scholars found that the formation of SUHIs in the western part declines towards the Northern and Southern parts of Colombo city (Emmanuel, 2005; Manawadu et al., 2008). Considering the administrative boundaries of Colombo, urban hot spots patterns changes in the west-to-east direction. However, these results were concluded based on two Landsat images (namely from 1997 and 2017) (Ranagalage et al., 2018). Though the cooling effect of sea breezing can control UHIs (Johansson et al., 2006), it is doubtful how this will be valid for rapidly constructing areas, like Colombo port city. In the current study, the focus is to identify UHI zones and UHS patterns with the help of LST data from 1988 to 2019. Here we use LST, NDVI, NDBI and UHS as parameters for each Landsat image. Current research can also provide a better understanding of the spatial and temporal dynamicity in the Colombo district.

## METHODS

The Study Area Colombo is a low landed district located in the western province of Sri Lanka, between $6^{\circ}42^{'}$ - $6^{\circ}58^{'}$ North latitude and $79^{\circ}50^{'}$ - $80^{\circ}13^{'}$ East longitude ranges (Fig. 1). It has two main monsoon seasons and two inter- monsoons and these monsoon seasons cause hot and humid climate changes (Ranagalage et al., 2018). The main monsoons blow southwest from late May to late September and from the northeast from late November to mid- February. During the inter-monsoon period (between March and May) temperatures are at their peak levels (Johansson et al., 2006). The mean annual rainfall is about 2300 $mm$ and

average annual temperature is 28 ℃ (Ranagalage et al., 2017). Thus, the season from December to early March is identified as the driest season of the Colombo district.

Higher rate of population, artificial surfaces, and low vegetation cover are the main characteristics of this region (Manawadu et al., 2008). Most recent studies have shown these characteristics lead to the formation of UHIs.

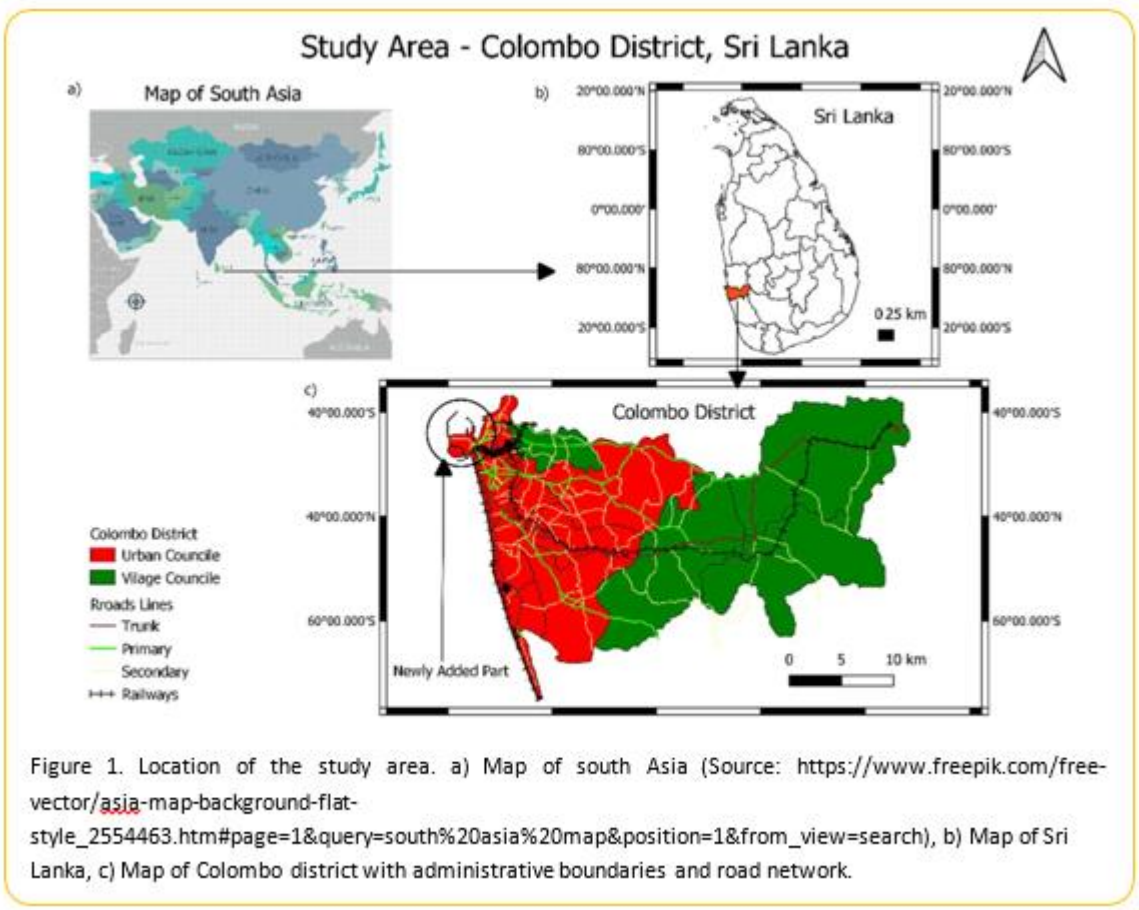


Figure 1. Location of the study area. a) Map of south Asia (Source: https://www.freepik.com/free-vector/asia-map-background-flat-style_2554463.htm#page=1&query=south%20asia%20map&position=1&from_view=search), b) Map of Sri Lanka, c) Map of Colombo district with administrative boundaries and road network.

## Landsat Images

The Landsat-5 TM and Landsat-8 OLI/TIRS satellite images were used to derive the LST, NDVI and NDBI. The Landsat satellite images are freely available to download on the United States Geological Services (USGS) website (http://earthexplorer.usgs.gov/). These images were acquired during the dry season of the Colombo district. The following Table 1 represents the details of Landsat images that were used in this study.

**Table 1. Information of Landsat images**

| | | | | Landsat |
|---|---|---|---|---|
| Date | Time | Cloud Cover (%) | Cloud Cover Land (%) | |
| | | | Version | |
| 12/15/1988 | 04:24:16.1930250Z | 8 | 8 | L05 |
| 2/7/1997 | 04:18:38.1820130Z | 8 | 8 | L05 |

| | | | | |
|---|---|---|---|---|
| 1/2/2007 | 04:48:43.2450750Z | 23 | 26 | L05 |
| 1/8/2015 | 04:53:58.6950720Z | 3.21 | 3.34 | L08 |
| 1/13/2017 | 04:54:05.6817070Z | 2.89 | 3.03 | L08 |
| 1/3/2019 | 04:53:47.7145259Z | 16.9 | 17.63 | L08 |

## Image Preprocessing

The Landsat-5 TM and Landsat-8 OLI/TIRS projects satellite images were used to analyze the spatial changes of biophysical parameters. Firstly the images have to be corrected radiometrically and atmospherically to enhance their quality using the QGIS Desktop 3.16.0 software. The Landsat- 8 OLI/TIRS thermal infrared band (band 10) has 100 m resolution and Landsat- 5 TM thermal-infrared band (band 6) has a resolution of 120 m. These thermal images were resampled using the nearest-neighbor algorithm with a pixel size of 30 m to match the optical bands. All of these preprocessing steps (Fig. 2) were done in WGS84/UTM 44 N projection coordinate system. After prepressing, Fig. 3 shows the NDVI, NDBI, LST, UHI and UHS zones derivation steps of this paper.

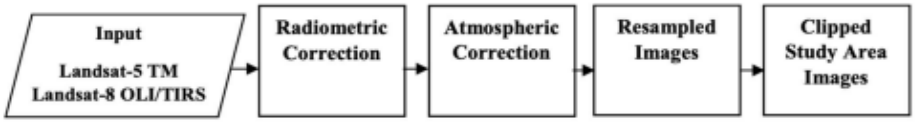


**Figure 2.** Image preprocessing steps.

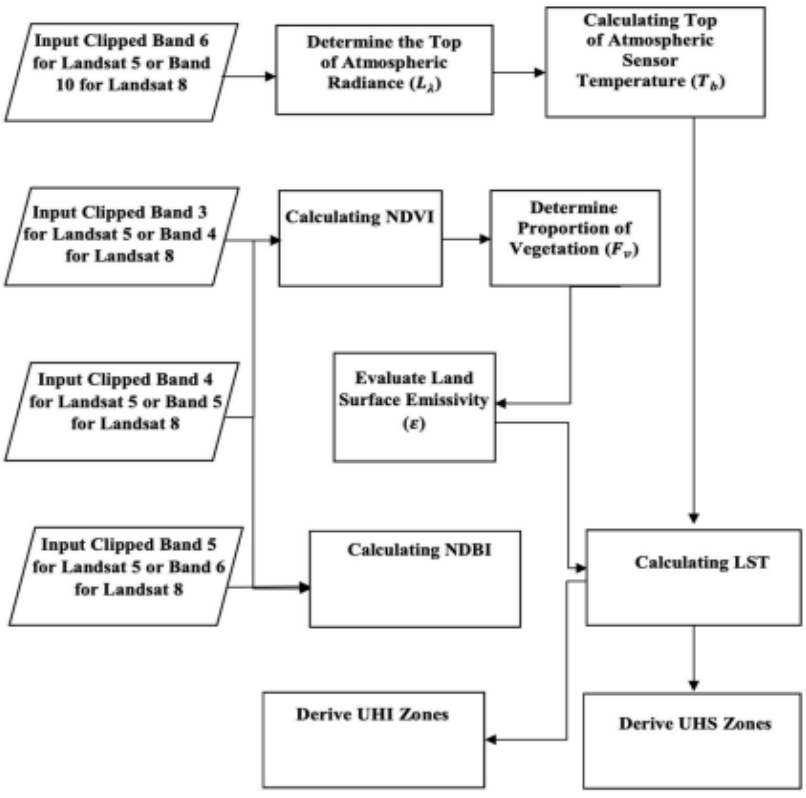


**Figure 3.** Flowchart for NDVI, NDBI, LST UHI and UHS zones derivation.

**Extraction of LU-LC distribution of NDVI and NDBI**

Calculating NDVI

NDVI is a useful parameter to classify urban vegetation (Chen et al., 2006). The NDVI lies between -1 to +1. Positive NDVI values represent vegetation, and negative or more close to zero values represent water bodies (Avdan & Jovanovska, 2016; Zaitunah et al., 2018; Ranagalage et al., 2018). This index is formulated as below (Guha et al., 2020)

Where

$$NDVI \quad \frac{(NIR - RED)}{(NIR + RED)} \qquad (1)$$

For Landsat 5 TM, NIR (Near-infrared) = band 4 and RED = band 3; for Landsat 8 OLI, NIR (Near-infrared) = band 5 and RED = band 4

Calculating NDBI

The NDBI lies between -1 to +1. In this range, values closer to 0 represent vegetation cover; negative values represent water bodies, and positive values for built-up areas ( Ranagalage et al., 2018; Zha et al., 2003) NDBI is used to identify urban and built-up areas (Chen et al., 2006).

Where

$$NDBI = \frac{(MIR - NIR)}{(MIR + NIR)} \qquad (2)$$

For Landsat 5 TM, MIR (Mid-infrared) = band 5 and NIR (Near-infrared) = band 4; for Landsat 8 OLI, MIR (Mid- infrared) = band 6 and NIR (Near-infrared) = band 5

LST from Landsat data

This LST retrieving algorithm is based on converting thermal bands' DNs into radiance values. And these radiances are used to evaluate the sensor brightness temperatures.

Determining Top of Atmospheric Radiance (Lλ)

The following two equations were used to convert the DN values of thermal bands to spectral radiance values of Landsat 5 and Landsat 8 images (Artis et al., 1982; U.S. Geological Survey, 2016).

For Landsat 5 TM thermal band (band 6):

$$L\lambda = 0.0056322 * DN + 0.1238 \qquad (3)$$

For Landsat 8 OLI thermal band (band 10):

$$L\lambda = 0.0003342 * DN + 0.1 \qquad (4)$$

Where

$L\lambda$ is the spectral radiance in $Wm^{-2}sr^{-1}mm^{-1}$

Calculating Top of Atmospheric Sensor Temperature ($T_b$)

To retrieve the sensor brightness temperature in Celsius from spectral radiance values, the following equation was used (Avdan et al., 2016).

$$T_b = \frac{K_2}{ln[(K_1/L_\lambda) + 1]} - 273.15 \quad (5)$$

Where

$T_b$ is the brightness temperature in Celsius(℃), $L\lambda$ is the spectral radiance in $Wm^{-2}sr^{-1}mm^{-1}$; $K_1$ and $K_2$ are calibration constants. For Landsat 5 TM $K_1 = 607.76$ and $K_2 = 1260.56$; For Landsat 8 OLI $K_1 = 774.89$ and $K_2 = 1321.08$

Determine Proportion of Vegetation ($F_V$)

The NDVI thresholds methodology (Sobrino et al., 2004) was used to calculate the land surface emissivity (ε). The fractional vegetation($F_V$) of each pixel was calculated by following expression.

$$F_v = \left(\frac{NDVI - NDVI_{min}}{NDVI - NDVI_{max}}\right)^2 \quad (6)$$

Where
$NDVI - NDVI_{\max}$

NDVI is the normalized difference vegetation index. The $NDVI_{min}$ and $NDVI_{max}$ are the minimum and maximum values of the NDVI, respectively.

Evaluate Land Surface Emissivity (ε)

dε is the effect of the geometrical distribution of the natural surfaces and internal reflections. For heterogeneous and undulating surfaces, the value of dε may be 2%.

$$d\varepsilon = (1 - \varepsilon_S)(1 - F_V)F\varepsilon_V \quad (7)$$

Where

$\varepsilon_V$ is vegetation emissivity, $\varepsilon_S$ is soil emissivity, $F_V$ is fractional vegetation and F is a shape factor whose mean is
0.55 (Sobrino et al., 2004).

$$\varepsilon = \varepsilon_V F_V + \varepsilon_S(1 - F_V) + d\varepsilon \quad (8)$$

Where

**ε** is emissivity.

**ε** gives (Sobrino et al., 2004) the following equation:

$$\varepsilon = 0.004F_V + 0{:}\,986 \quad (9)$$

Calculating LST

Hence, the **LST** was derived as follow (Guha, 2017; Guha et al., 2018; Ranagalage et al., 2018)

$$LST = \frac{T_B}{1 + (\lambda\sigma T_B/hc)ln\varepsilon} \quad (10)$$

Where

λ is the effective wavelength (λ = 11.5 μm for Landsat TM Band 6, λ = 10.8 μm for Landsat TIRS Band 10), σ is Boltzmann constant ($1.38 \times 10^{-23}$ $JK^{-1}$), h is Plank's constant ($6.626 \times 10^{-34}$ Js), c is the velocity of light in a vacuum($2.998 \times 10^{-8}$ $ms^{-1}$) and ε is emissivity.

Mapping Urban Heat Island and Non- Urban Heat Island Zones

The following two expressions were used to map the Urban Heat Island areas and Non-Urban Heat Island areas for different years (Guha, 2017; Guha et al., 2018).

For UHI Zones

$$LST > \mu + 0.5 * \delta \quad (11)$$

And for Non-UHI Zones

$$0 < LST \leq \mu + 0.5 * \delta \quad (12)$$

Where

μ is the mean LST and δ is the standard deviation of LST.

Delineating the Urban Hot Spots

The following expression was used to find the UHS from LST maps in the Colombo district over different years (Guha, 2017; Guha et al., 2018). These UHS are extremely hot and generate inside the UHI zones. It is not recommended for human settlements in these hot pocket areas.

$$LST > \mu + 2 * \delta \quad (13)$$

Statistical Analysis

Finally to observe the LST variations with respect to the other biophysical parameters, linear regression models were adopted. These statistical analysis were done using the RStudio an open source software.

## RESULTS AND DISCUSSION

Spatial changes of LST, NDVI, and NDBI over time

Dynamicity of LST

**Table 2. Land Surface Temperature summary in Celsius.**

| | | | | LST(°C) | | |
|---|---|---|---|---|---|---|
| Year | Min | Max | Mean | Sd | Threshold Temperature for UHI | Threshold Temperature for UHS |
| 1988 | 15.642 | 28.768 | 22.291 | 1.176 | 22.879 | 24.643 |
| 1997 | 21.503 | 34.860 | 26.914 | 1.137 | 27.483 | 29.188 |
| 2007 | 10.926 | 34.063 | 26.926 | 2.142 | 27.997 | 31.210 |
| 2015 | 23.148 | 34.675 | 26.464 | 1.391 | 27.160 | 29.246 |
| 2017 | 22.500 | 33.821 | 27.005 | 1.585 | 27.798 | 30.175 |
| 2019 | 23.377 | 35.801 | 27.343 | 1.641 | 28.164 | 30.625 |

As per Table 2, LST varied from 15.642℃ - 28.768℃ in 1988, 21.503℃ - 34.860℃ in 1997, 10.926℃ - 34.063℃ in 2007, 23.148℃ - 34.675℃ in 2015, 22.500℃ - 33.821℃ in 2017 and 23.377℃ - 35.801℃ in 2019. The mean of LST changed by 22.66% from 1988 to 2019. In 2007, it had an LST anomaly with a 2.142 standard deviation due to its highest cloud cover (Table 1). Furthermore, it shows the enhancing tend of the standard deviation of LST from 1997 to 2019 except 2007.

The derived LST images are shown in Fig. 4. Since we used the same color ramp, 99.93% of the area was less than 27℃ (<27℃) in 1988. Combining its' both lower mean of LST (Table 1) and the higher presentage of lower LST area, 1988 was the coolest year. In 1997, and 2007, high LST lands were mostly noticeable adjacent to the Colombo harbour area (Fig. 4). This fact has been previously notified in several studies (Manawadu et al., 2008; Ranagalage et al., 2017, 2018). However, these lands had rapidly expanded towards the northern, southern, and eastern parts of the district by 2015. After 2007, the "Seethagama" which is located at the north-eastern boundary of the Colombo has been generating a high LST area following the spatial dynamicity of the urban construction area.

### Dynamicity of NDVI and NDBI

Table 3 shows a descriptive summary of NDVI values of the Colombo district. The NDVIs ranged from -0.372 to 0.780 in 1988, -0.415 to 0.810 in 1997, -0.228 to 0.767 in 2007, -0.388 to 0.832 in 2015, -0.245 to 0.804 in 2017
and -0.443 to 0.832 in 2019. The mean of NDVI positively increased from 0.516 to 0.561. As Fig. 5, greenery areas with high NDVIs represent more vegetated and cultivated lands. The gross deforestation of Colombo district in 1992-1996 was 118 $ha\ \ yr^{-1}$ and also rice paddy extent of both irrigated and rainfed lands were 24 $ha\ \ yr^{-1}$ and –2 $ha\ \ yr^{-1}$ during this period respectively (Mattsson et al., 2012). The deforestation and cultivation of Colombo haven't been well-documented yet. However, Fig. 5 shows an improvement of vegetation cover in the eastern part of Colombo from 1988 - to 2019. Hence, it implies that rate changes of cultivation can mitigate some amount of deforestation impaction.

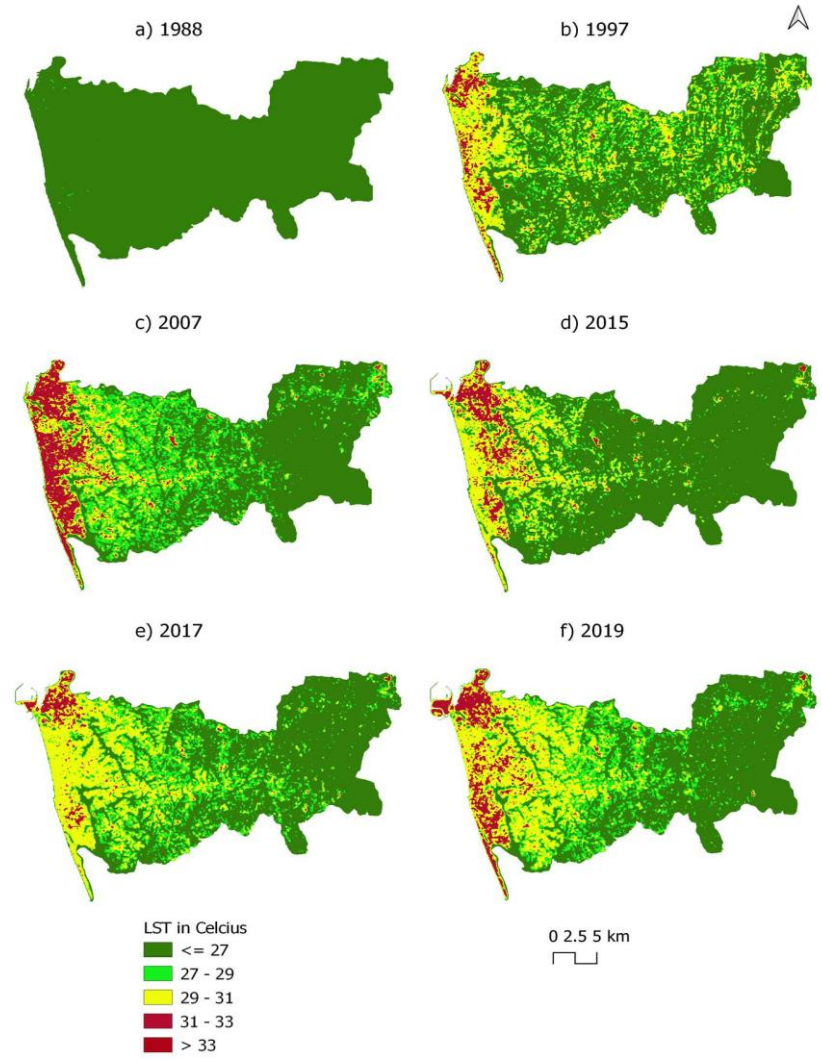


Figure 4. The spatial patterns of LST a) 1988, b) 1997, c) 2007, d) 2015, e) 2017 and f) 2019.

The NDBI maximum values were continually increasing from 1988 to 2019 (Table 3). Generally, built-up areas increased between 1988 and 2019; and this fact is noticeable in Fig. 6 In 1988, the highest NDBI values were distributed along with the western coastal belt and adjacent to the western part of the area. But this distribution was getting expanded to the north, east, and south along with transporting system and constructed areas. In 2015, 2017, and 2019 images, the highest NDBI values were located adjacent to the newly added part of the district. The port city project was initiated during the 2014 – 2015 period after many political and public acceptance (De Silva et al., 2015; Dias et al., 2016) and this explains the highest NDBI values abounded in the port city area.

**Table 3. NDVI and NDBI of 1988,1997,2015,2017 and 2019.**

| | | NDVI | | | | | NDBI | | |
|---|---|---|---|---|---|---|---|---|---|
| Year | Min | Max | Mean | Sd | Min | Max | | Mean | Sd |
| 1988 | -0.372 | 0.780 | 0.516 | 0.153 | -0.630 | 0.383 | | -0.262 | 0.107 |
| 1997 | -0.415 | 0.810 | 0.494 | 0.150 | -0.740 | 0.378 | | -0.222 | 0.127 |
| 2007 | -0.228 | 0.767 | 0.481 | 0.144 | -0.641 | 0.325 | | -0.211 | 0.118 |
| 2015 | -0.388 | 0.832 | 0.588 | 0.166 | -0.629 | 0.364 | | -0.156 | 0.136 |
| 2017 | -0.245 | 0.804 | 0.528 | 0.160 | -0.578 | 0.359 | | -0.162 | 0.133 |
| 2019 | -0.443 | 0.832 | 0.561 | 0.178 | -0.622 | 0.404 | | -0.181 | 0.142 |

**Figure 5. NDVI of a) 1988, b) 1997, c) 2007, d) 2015, e) 2017 and f) 2019.**

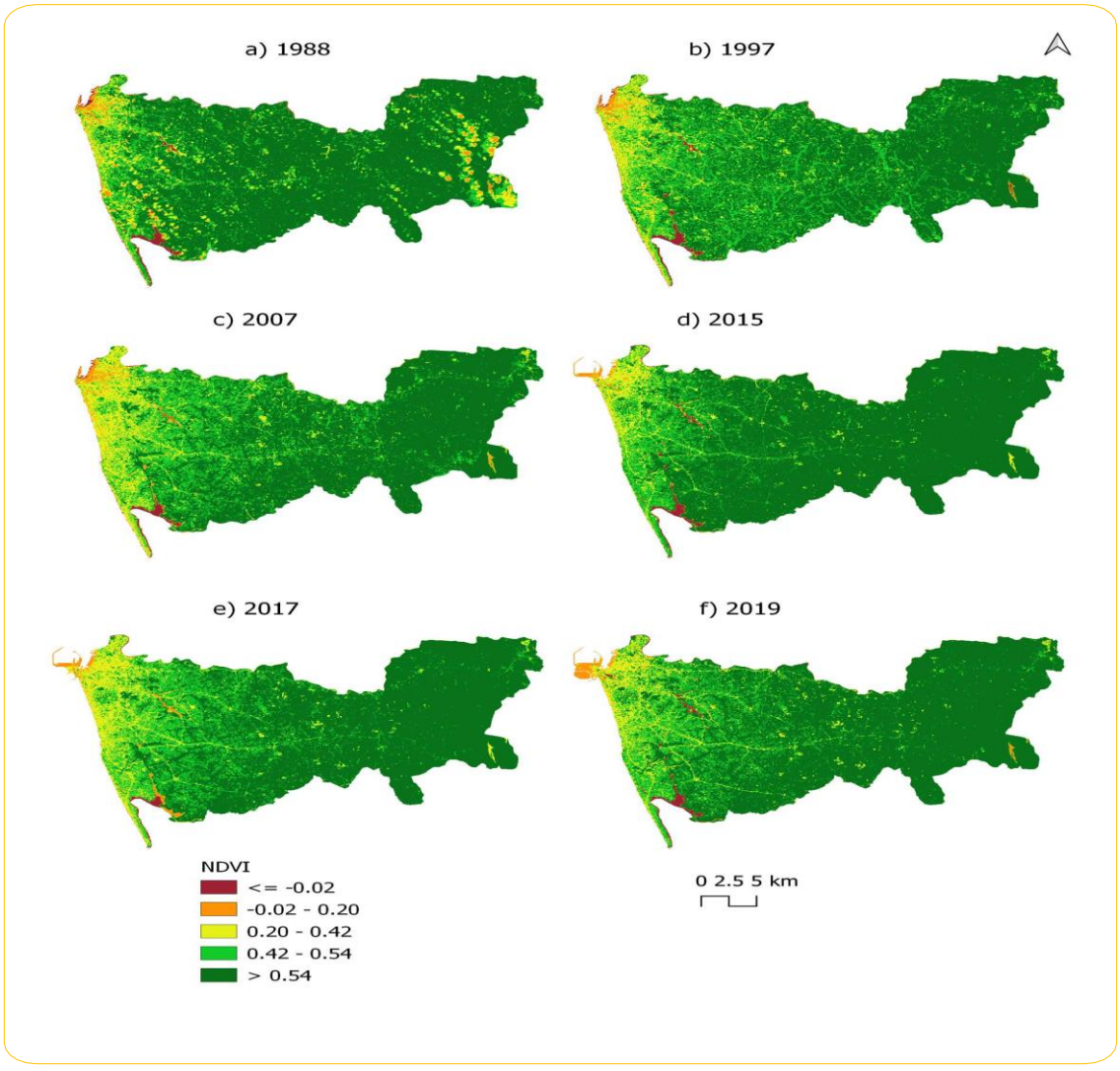

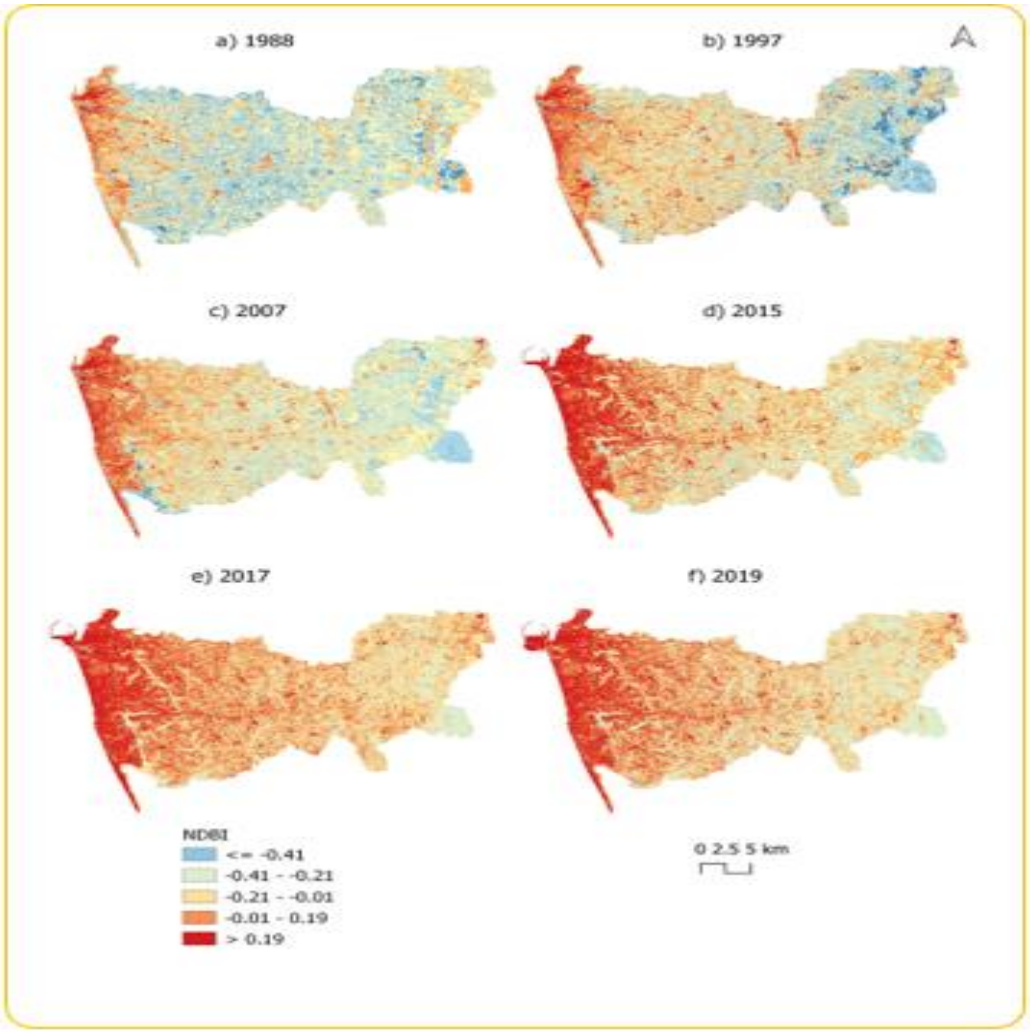


**Figure 6. NDBI of a) 1988, b) 1997, c) 2007, d) 2015, e) 2017 and f) 2019.**

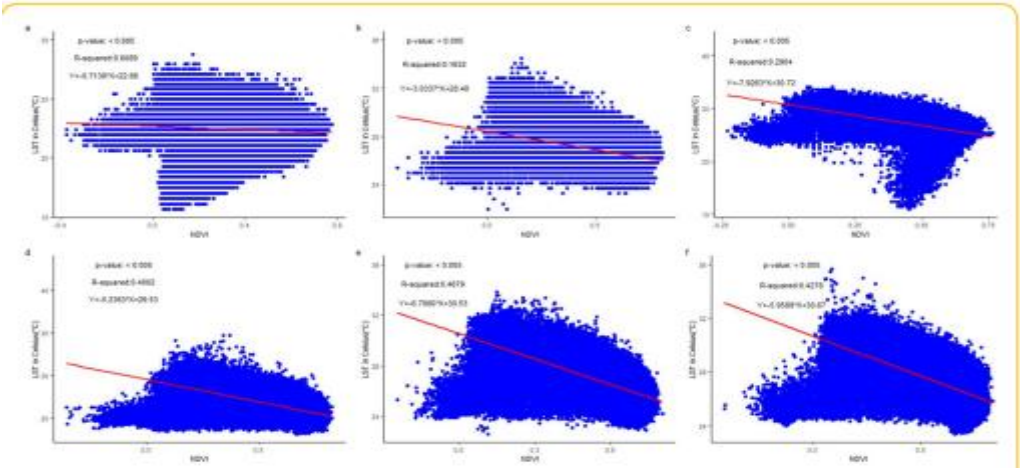

**Figure 7.** Scatter plots between LST and NDVI a) 1988, b) 1997, c) 2007, d) 2015, e) 2017, f) 2019.

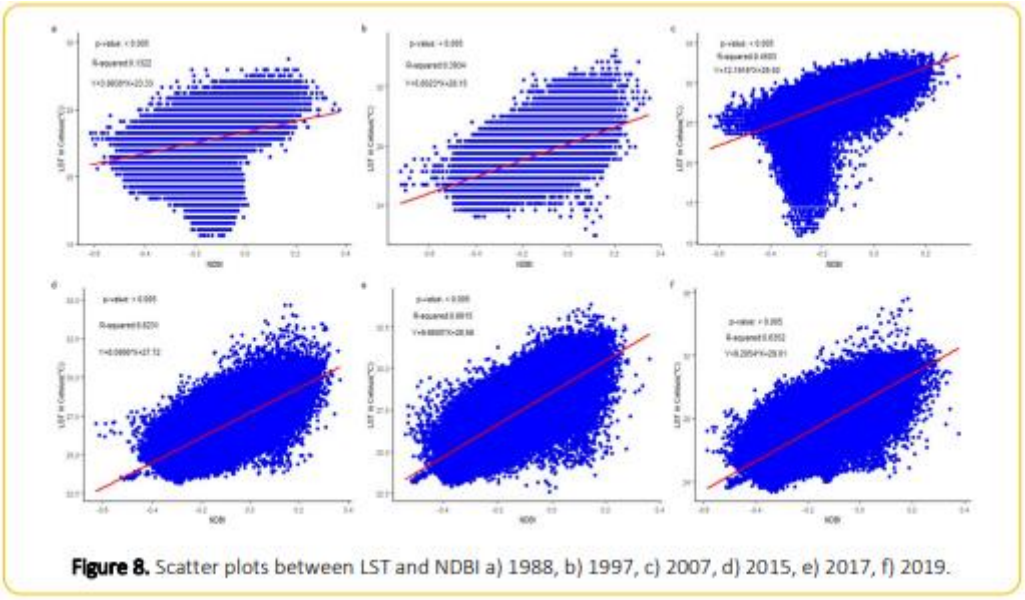

**Figure 8.** Scatter plots between LST and NDBI a) 1988, b) 1997, c) 2007, d) 2015, e) 2017, f) 2019.

LST has a negative relationship with vegetation cover and it has an inverse relationship with built-up areas and bare lands. For each year, p-values are less than 0.005 (Fig. 7 & Fig. 8) while NDVI and NDBI have statistically significant relationships between LSTs. In 1988, the correlation between NDVI and LST was low due to its' less urbanization. Generally, NDBI vs. LST is a much stronger relationship than NDVI vs. LST. It concludes the predictive modelling or explanatory modelling power of NDBI affects on the much stronger way on LST than NDVI. The increasing trend of $R^2$ (Table 4) in both NDVI and NDBI interpret that spatial change of LST were getting stronger in 1988,1997,2007,2015,2017 and 2019 as the Colombo become more urbanized.

**Table 4. Correlation coefficients and R squares of NDVI and NDBI with respect to LST.**

**Table 4.** Correlation coefficients and R squares of NDVI and NDBI with respect to LST.

| Biophysical Parameter and $R^2$ values | 1988 | 1997 | 2007 | 2015 | 2017 | 2019 |
|---|---|---|---|---|---|---|
| NDVI | -0.7183 | -3.0337 | -7.9263 | -5.2363 | -6.7080 | -5.9589 |
| $R^2$ | 0.0089 | 0.1632 | 0.2904 | 0.4002 | 0.4679 | 0.4278 |
| NDBI | 3.9930 | 5.6023 | 12.1916 | 8.0906 | 9.6600 | 9.2054 |
| $R^2$ | 0.1322 | 0.3439 | 0.4503 | 0.6231 | 0.6651 | 0.6352 |

*UHI Zones patterns variations*

**Table 5. Temporal distribution of LST in UHI Zones.**

| Year | LST (Min) (°C) | | LST (Max) (°C) | | LST (Mean) (°C) | | LST (Sd) | | Area ($km^2$) | |
|---|---|---|---|---|---|---|---|---|---|---|
| | UHI | Non-UHI | UHI | Non-UHI | UHI | Non-UHI | UHI | Non-UHI | UHI | Non-UHI |
| 1988 | 22.879 | 15.642 | 28.768 | 22.879 | 23.942 | 21.921 | 0.785 | 0.898 | 125.043 | 557.660 |
| 1997 | 27.483 | 21.503 | 34.860 | 27.483 | 28.373 | 26.384 | 0.887 | 0.651 | 182.855 | 499.848 |
| 2007 | 27.997 | 10.926 | 34.063 | 27.997 | 29.571 | 26.512 | 0.928 | 1.873 | 169.598 | 513.105 |
| 2015 | 27.160 | 23.148 | 34.675 | 27.160 | 28.302 | 25.723 | 0.803 | 0.742 | 195.705 | 487.958 |
| 2017 | 27.798 | 22.500 | 33.821 | 27.798 | 28.514 | 26.131 | 0.936 | 0.982 | 212.878 | 471.308 |
| 2019 | 28.164 | 23.377 | 35.801 | 28.164 | 29.381 | 26.412 | 0.797 | 0.938 | 214.512 | 471.844 |

The UHI intensity is interpreted as the mean temperatures difference between UHI and Non-UHI areas. The temporal distribution of derived LSTs for UHI and Non-UHI zones are shown in Table 5. UHI intensities fluctuate with increasing order. The UHI intensities were 2.021°C, 1.989°C, 3.059°C, 2.579°C, 2.383°C and 2.969°C in 1988, 1997, 2007, 2015, 2017 and 2019 respectively. The standard deviation of UHI areas explain the clear picture of the UHI intensity of Colombo, i.e. 0.785 in 1988, 0.887 in 1997, 0.928 in 2007, 0.803 in 2015, 0.936 in 2017 and 0.797 in 2019. It implies that UHI intensity was consistent throughout the UHI for various Landsat projects. The expansion of UHI zones area was 71.55% from 1988 to 2019 and is evidence of a rapid increase of SUHI phenomena in the study area. And these UHI zones expanded from the western coastal belt to the eastern along with the center part of the district is observed from Fig. 9.

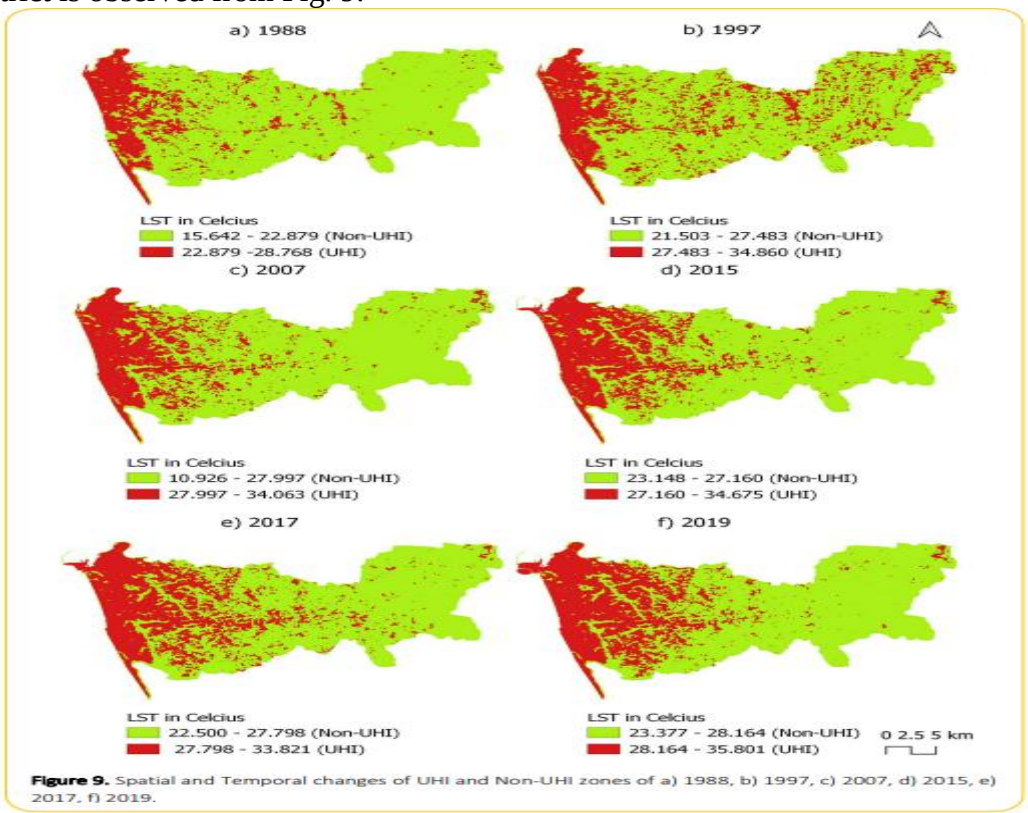


**Figure 9.** Spatial and Temporal changes of UHI and Non-UHI zones of a) 1988, b) 1997, c) 2007, d) 2015, e) 2017, f) 2019.

Figure 9. Spatial and Temporal changes of UHI and Non-UHI zones of a) 1988, b) 1997, c) 2007, d) 2015, e) 2017, f) 2019.

**Table 6. Temporal Distribution of LST in UHS Zones**

| | UHS Zones | | | |
|---|---|---|---|---|
| Year | Threshold Temperature for UHS(℃) | Maximum Temperature(℃) | Non-UHS Area($km^2$) | UHS Zones Area ($km^2$) |
| 1988 | 24.643 | 28.768 | 665.276 | 17.427 |
| 1997 | 29.188 | 34.860 | 659.582 | 23.121 |
| 2007 | 31.210 | 34.063 | 672.433 | 10.270 |
| 2015 | 29.246 | 34.675 | 658.746 | 24.917 |
| 2017 | 30.175 | 33.821 | 669.780 | 14.405 |
| 2019 | 30.625 | 35.801 | 671.951 | 14.405 |

The main goal of this study is to identify the UHS pattern based on Landsat data. These hot pockets are developed inside the UHI zones and they aren't recommended for human settlements. In 1988 and 1997, urban hot spots were founded to be declining along with the western coastal belt. However, after 2015, they were more concentrated and adjacent to the port city area (Fig. 10). These UHS were observed by threshold temperature (Table 6). Additionally, other new hot spots have been generating since 2017 around "Seethagama" and also this zone is recognized as ongoing construction projects area. As in earlier studies, areas close to bare land, parking areas and construction fields have a higher possibility of generating UHS and this fact is supported by our final findings. Low vegetation and water bodies' distribution are a recognizable common matter in these zones. Fig. 11 shows the gradual increase of the threshold temperature in both UHI and UHS zones during the past 3 decades. Thus, we can expect much more heat pockets in near future adjacent to highly industrial sites in the Colombo district.

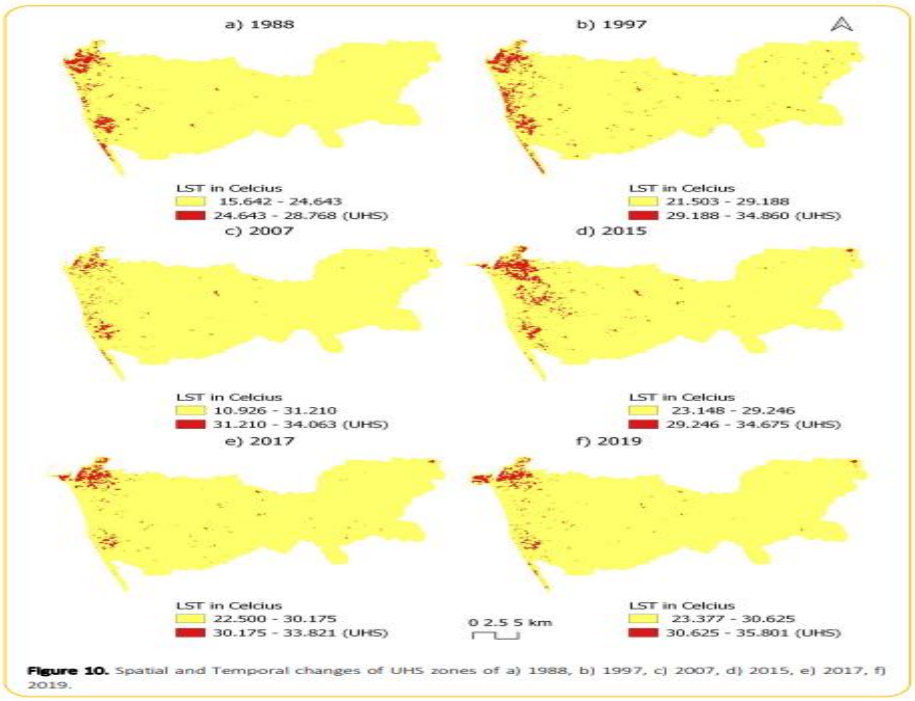


**Figure 10.** Spatial and Temporal changes of UHS zones of a) 1988, b) 1997, c) 2007, d) 2015, e) 2017, f) 2019.

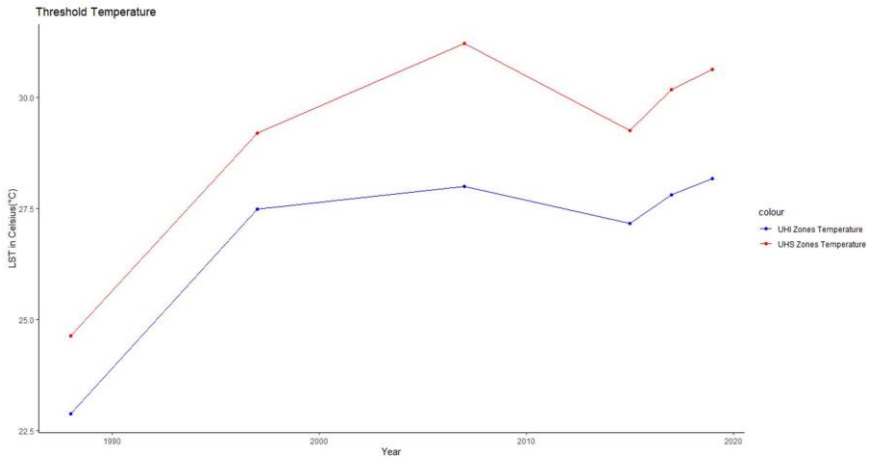


Figure 11. Line graph of Threshold LST variation for UHI

## CONCLUSIONS

In this study, multiple Landsat images for 1988, 1997, 2007, 2015, 2017, and 2019 were used to study the dynamicity of the urban heat island scenario of the Colombo district in Sri Lanka. The result revealed that earlier, these UHI zones were located in the western coastal belt; however, they were expanded to the eastern along with the center part of the district during the past 3 decades. Furthermore, the expansion of UHI zones area was 71.55% from 1988 to 2019 and is an evidence of a rapid increase of SUHI phenomena in the study area.

For the main objective of this study, even though hot spots had declined along with the western coastal belt in prior years, in 2019, these spots were found to be more concentrated and adjacent to the port city area. In addition, there are new hot spots that have been generating since 2017 around "Seethagama", which is a construction project area. A gradual increase of threshold temperature in both UHI and UHS zones during the past 3 decades explains that it can be predicted much more heat pockets in near future adjacent to highly industrial sites in the Colombo district.

Hence, these observations could be helpful to aid in mitigating these micro-climatic effects in the Colombo district. There is an urgent need for urban designers and policymakers to pay attention to this situation. According to previous research, it is highly recommended that urban greening strategies are adopted to control the generation of UHI and UHS zones.

In the future, more work can be done to elaborate the findings of this paper. Other method or remotely sensed satellite images can be used to validate current findings. Additional biophysical parameters can also be added to increase the quality of results. Application of advanced statistical methods to estimate correlations between parameters used can also be done. Finally, a model can be built to predict future scenarios and outcomes of LST variations changes over time.

## Acknowledgments

The researchers gratefully thank two anonymous reviewers for providing their valuable comments and suggestions on this study. They are also indebted to the USGS web server (http://earthexplorer.usgs.gov/).

**References**

1. Amiri, R., Weng, Q., Alimohammadi, A., & Alavipanah, S. K. (2009). Spatial-temporal dynamics of land surface temperature in relation to fractional vegetation cover and land use/cover in the Tabriz urban area, Iran. Remote Sensing of Environment, 113(12), 2606–2617. doi: 10.1016/j.rse.2009.07.021
2. Artis, D. A., & Carnahan, W. H. (1982). Survey of emissivity variability in thermography of urban areas. 313–329. doi: 10.1016/0034-4257(82)90043-8
3. Avdan, U., & Jovanovska, G. (2016). Algorithm for automated mapping of land surface temperature using LANDSAT 8 satellite data. Journal of Sensors, 2016. doi: 10.1155/2016/1480307
4. Barsi, J. A., Hook, S. J., Palluconi, F. D., Schott, J. R., & Raqueno, N. G. (2006). Landsat TM and ETM+ thermal band calibration. Earth Observing Systems XI, 6296(September 2006), 62960F. doi: 10.1117/12.683212
5. Chen, L., Zhu, W., Zhou, X., & Zhou, Z. (2003). Characteristics of the heat island effect in Shanghai and its possible mechanism. In Advances in Atmospheric Sciences (Vol. 20, Issue 6, pp. 991–1001). doi: 10.1007/bf02915522
6. Chen, X. L., Zhao, H. M., Li, P. X., & Yin, Z. Y. (2006). Remote sensing image-based analysis of the relationship between urban heat island and land use/cover changes. Remote Sensing of Environment, 104(2), 133–146. doi: 10.1016/j.rse.2005.11.016
7. Coutts, A. M., White, E. C., Tapper, N. J., Beringer, J., & Livesley, S. J. (2016). Temperature and human thermal comfort effects of street trees across three contrasting street canyon environments. Theoretical and Applied Climatology, 124(1–2), 55–68. doi: 10.1007/s00704-015-1409-y
8. De Silva, S. U., Sachindrani, D., Hatharasinghe, H., & Bogahawatte, I. (2015). The Contradiction between Sustainable Development and Economic Development: Special Reference to the Colombo Port City Project of Sri Lanka. November, 196–201.
9. Dias, I., Perera, L., Bandara, S., & Lim, K. S. (2016). Review of internal and external transportation issues of artificial city developments: Port City, Colombo, Sri Lanka. ATRF 2016 - Australasian Transport Research Forum 2016, Proceedings, November.
10. Emmanuel, R. (2005). Thermal comfort implications of urbanization in a warm-humid city: The Colombo Metropolitan Region (CMR), Sri Lanka. Building and Environment, 40(12), 1591–1601. doi: 10.1016/j.buildenv.2004.12.004
11. Estoque, R. C., Murayama, Y., & Myint, S. W. (2017). Effects of landscape composition and pattern on land surface temperature: An urban heat island study in the megacities of Southeast Asia. Science of the Total Environment, 577, 349–359. doi: 10.1016/j.scitotenv.2016.10.195
12. Gerald, N., & Perera, R. (2015). CLIMATE - SENSITIVE URBAN PUBLIC SPACE : A SUSTAINABLE APPROACH TO URBAN HEAT ISLAND MITIGATION IN COLOMBO , SRI LANKA CLIMATE - SENSITIVE URBAN PUBLIC SPACE : A SUSTAINABLE APPROACH TO URBAN HEAT ISLAND MITIGATION IN COLOMBO , SRI LANKA. January.
13. Guha, S. (2017). Dynamic analysis and ecological evaluation of urban heat islands in Raipur city, India. Journal of Applied Remote Sensing, 11(03), 1. doi: 10.1117/1.jrs.11.036020
14. Guha, S., Govil, H., Dey, A., & Gill, N. (2018). Analytical study of land surface temperature with NDVI and NDBI using Landsat 8 OLI and TIRS data in Florence and Naples city, Italy. European Journal of Remote Sensing, 51(1), 667–678. doi: 10.1080/22797254.2018.1474494

15. Guha, S., Govil, H., & Diwan, P. (2020). Monitoring LST-NDVI Relationship Using Premonsoon Landsat Datasets. Advances in Meteorology, 2020(1). doi: 10.1155/2020/4539684

16. Guo, G., Wu, Z., Xiao, R., Chen, Y., Liu, X., & Zhang, X. (2015). Impacts of urban biophysical composition on land surface temperature in urban heat island clusters. Landscape and Urban Planning, 135, 1–10. doi: 10.1016/j.landurbplan.2014.11.007

17. Johansson, E., & Emmanuel, R. (2006). The influence of urban design on outdoor thermal comfort in the hot, humid city of Colombo, Sri Lanka. International Journal of Biometeorology, 51(2), 119–133. doi: 10.1007/s00484-006-0047-6

18. Kim, Y. H., & Baik, J. J. (2005). Spatial and temporal structure of the urban heat island in Seoul. Journal of Applied Meteorology, 44(5), 591–605. doi: 10.1175/JAM2226.1

19. Reducing Urban Heat Islands: Compendium of Strategies Urban Heat Island Basics. (2008). In Reducing urban heat islands: Compendium of strategies. U.S. Environmental Protection Agency. https://www.epa.gov/heat- islands/heat-island-compendium

20. Li, Y. Y., Zhang, H., & Kainz, W. (2012). Monitoring patterns of urban heat islands of the fast-growing Shanghai metropolis, China: Using time-series of Landsat TM/ETM+ data. International Journal of Applied Earth Observation and Geoinformation, 19(1), 127–138. doi: 10.1016/j.jag.2012.05.001

21. Liu, L., & Zhang, Y. (2011). Urban heat island analysis using the landsat TM data and ASTER Data: A case study in Hong Kong. Remote Sensing, 3(7), 1535–1552. doi: 10.3390/rs3071535

22. Manawadu, L., & Liyanage, N. (2008). Identifying Surface Temperature Pattern of the City of Colombo (Vol. 1, Issue 05). Retrieved from http://unfccc.int/resource/docs/

23. Mattsson, E., Persson, U. M., Ostwald, M., & Nissanka, S. P. (2012). REDD plus readiness implications for Sri Lanka in terms of reducing deforestation. 100, 29–40.

24. Ranagalage, M., Estoque, R. C., & Murayama, Y. (2017). An urban heat island study of the Colombo Metropolitan Area, Sri Lanka, based on Landsat data (1997-2017). ISPRS International Journal of Geo-Information, 6(7). doi: 10.3390/ijgi6070189

25. Ranagalage, M., Estoque, R. C., Zhang, X., & Murayama, Y. (2018). Spatial changes of urban heat island formation in the Colombo District, Sri Lanka: Implications for sustainability planning. Sustainability (Switzerland), 10(5). doi: 10.3390/su10051367

26. Rodriguez Lopez, J. M., Heider, K., & Scheffran, J. (2017). Frontiers of urbanization: Identifying and explaining urbanization hot spots in the south of Mexico City using human and remote sensing. Applied Geography, 79(December 2016), 1–10. doi: 10.1016/j.apgeog.2016.12.001

27. Sharma, R., & Joshi, P. K. (2014). Identifying seasonal heat islands in urban settings of Delhi (India) using remotely sensed data - An anomaly based approach. Urban Climate, 9, 19–34. doi: 10.1016/j.uclim.2014.05.003

28. Sobrino, J. A., Jiménez-Muñoz, J. C., & Paolini, L. (2004). Land surface temperature retrieval from LANDSAT TM 5.

29. Remote Sensing of Environment, 90(4), 434–440. doi: 10.1016/j.rse.2004.02.003

30. Sultana Parvin, N., & Abudu, D. (2017). Estimating Urban Heat Island Intensity using Remote Sensing Techniques in Dhaka City.

31. Tan, J., Zheng, Y., Tang, X., Guo, C., Li, L., Song, G., Zhen, X., Yuan, D., Kalkstein, A. J., Li, F., & Chen, H. (2010). The urban heat island and its impact on heat waves and human health in Shanghai. International Journal of Biometeorology, 54(1), 75–84. doi: 10.1007/s00484-009-0256-x

32. U.S. Geological Survey. (2016). Landsat 8 Data Users Handbook. Nasa, 8(June), 97. Retrieved from https://landsat.usgs.gov/documents/Landsat8DataUsersHandbook.pdf

33. Yang, L., Qian, F., Song, D. X., & Zheng, K. J. (2016). Research on Urban Heat-Island Effect. Procedia Engineering, 169, 11–18. doi: 10.1016/j.proeng.2016.10.002

34. Yuan, F., & Bauer, M. E. (2007). Comparison of impervious surface area and normalized difference vegetation index as indicators of surface urban heat island effects in Landsat imagery. Remote Sensing of Environment, 106(3), 375–386. doi: 10.1016/j.rse.2006.09.003

35. Zaitunah, A., Samsuri, S., Ahmad, A. G., & Safitri, R. A. (2018). Normalized difference vegetation index (ndvi) analysis for land cover types using landsat 8 oli in besitang watershed, Indonesia. IOP Conference Series: Earth and Environmental Science, 126(1). doi: 10.1088/1755-1315/126/1/012112

36. Zha, Y., Gao, J., & Ni, S. (2003). Use of normalized difference built-up index in automatically mapping urban areas from TM imagery. International Journal of Remote Sensing, 24(3), 583–594. doi: 10.1080/01431160304987

37. Zhang, J., & Yao, F. (2009). The characteristics of urban heat island variation in beijing urban area and its impact factors. 2009 Joint Urban Remote Sensing Event, 1–6. doi: 10.1109/URS.2009.5137502